RSC Advances

ROYAL SOCIETY OF CHEMISTRY

www.rsc.org/advances

Graphical Abstract

A facile Eco-friendly attempt was made to fabricate antibacterial nanocomposite hydrogels of Au-core Ag-shell nanoparticles separately from medically importance gained Carbopol® 980 NF and Noveon® AA-1 Polycarbophil polymers by nucleation of Au^{3+} and Ag^{+} ions from the extracts of naturally available mint leaves. The developed nanocomposite hydrogels possess excellent antibacterial and swelling properties. Hence, from the viewpoint of applications, the developed Au-core Ag-shell nanocomposite hydrogels may be used for superior biomedical applications ranging from transdermal wound dressing materials to sanitary appliances.

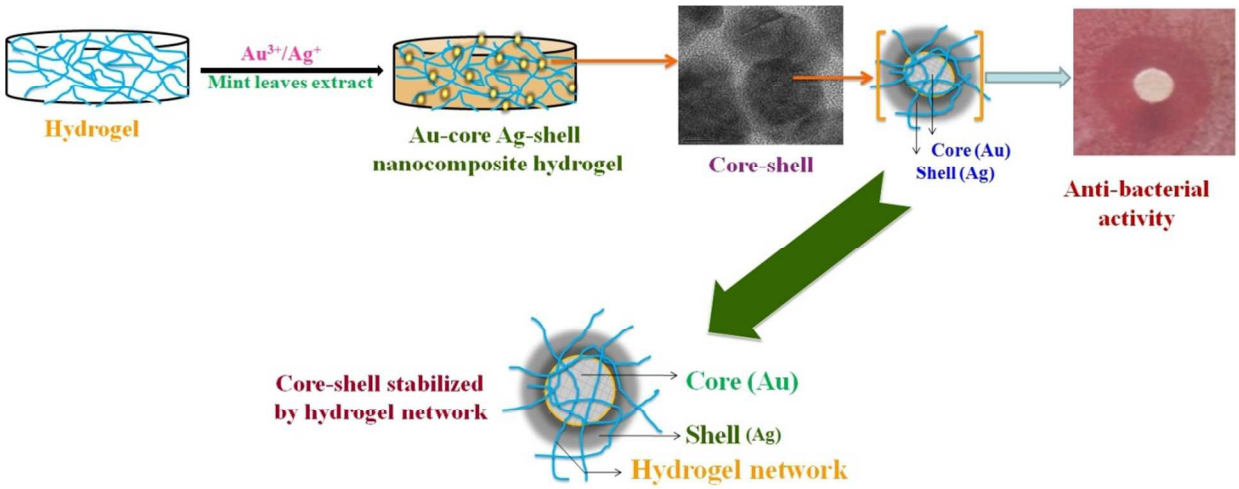

Synthesis route for fabrication of Au-core Ag-shell nanocomposite hydrogel

Antibacterial Nanocomposite Hydrogels for Superior Biomedical Applications: A Facile Eco-Friendly Approach

Gownolla Malegowd Raghavendra[1*], Tippabattini Jayaramudu[1], KokkarachedуVaraprasad[2*], Goddeti Siva Mohan Reddy[3], Konduru Mohana Raju[1]

1. Synthetic Polymer Laboratory, Department of Polymer Science & Technology, Sri Krishnadevaraya University, Anantapuramu- 515003, A. P, India.
2. Center for Advanced Polymer Research, CIPA, Beltran Mathieu 224, Floor 2, Concepción, Chile.
3. Department of Applied Chemistry, University of Johannesburg, Doornfontein 2028, Johannesburg, South Africa.

*Corresponding authors:
Dr. KokkarachedуVaraprasad
Center for Advanced Polymer Research, CIPA, Beltran Mathieu 224, Floor 2, Concepción, Chile.
E-mail: varmaindian@gmail.com, prasad@cipachile.cl
and
GownollaMalegowdRaghavendra
Synthetic Polymer Laboratory,
Department of Polymer Science & Technology,
Sri Krishnadevaraya University,
Anantapuramu- 515003, A. P, India.
E-mail: gmraghavendrasku@gmail.com

Abstract

In this scientific paper, we report a facile and eco-friendly fabrication of antibacterial nanocomposite hydrogels of Au-core Ag-shell nanoparticles, embedded within Carbopol® 980 NF/ Noveon® AA-1 Polycarbophil acrylic acid polymeric matrix. The aim of the study was to investigate whether the nanocomposite hydrogels have the potential to be used for bacterial inactivation applications. The key feature was that unlike the use of chemical reductants, auxiliary stabilizers and specialized expensive equipment, the possible Au-core Ag-shell nanoparticles (~15 ± 3 nm) were synthesized by utilizing aqueous mint leaves' extracts. The developed hydrogels were characterized by fourier transform infrared spectroscopy, transmission

electron microscopy, scanning electron microscopy-energy dispersive spectroscopy and thermo gravimetric analysis. Swelling studies were performed in phosphate buffered saline, pH 7.4 solution. A sustained antibacterial study against *E.coli* (G -) and *B. subtilis* (G +), showed their excellent antibacterial efficiency, which suggested that the developed hydrogels were potential candidates for wide range of biomedical applications.

Keywords: Eco-friendly fabrication; Antibacterial nanocomposite hydrogels; Carbopol® 980 NF; Noveon® AA-1 Polycarbophil; Au-core Ag-shell nanoparticles; Mint leaves.

Introduction

Rapid growth of materials science has provided many types of functional materials for biomedical applications. One such type of functional material is hydrogel [1-6]. Hydrogels are three-dimensional (3D), hydrophilic polymeric networks capable of imbibing large amounts of water or biological fluids [7,8] and resemble like natural living biological tissue more than any other class of synthetic biomaterials due to their high water contents and can provide a better feeling for the skin in comparison to conventional ointments and patches [9]. These well-defined characteristic properties offered researchers to utilize hydrogels for various biomedical applications which include, production of wound dressing materials, trans-dermal systems, drug delivery carriers, sanitary pads, disposable diapers, dental materials, implants, injectable polymeric systems, ophthalmic applications and hybrid-type organs (encapsulated living cells) [10-14].

In generally, hydrogels are being synthesized from raw materials of either natural or synthetic origin. Over the last two decades, significant modifications have been revolutionized for comprehensive applications of hydrogels in almost all fields. This gradually replaced ‘natural based hydrogels’ by ‘synthetic based hydrogels’ [15]. The present research work is one such,

aimed to fabricate antibacterial hydrogels from commercially available acrylic acid polymers: Carbopol® 980 NF (acrylic acid polymers cross-linked with allyl ethers of pentaerythritol) and Noveon® AA-1 Polycarbophil (acrylic acid polymer crosslinked with divinyl glycol) [16,17]. The available literature pertaining to these materials is very less. Among the available literature Carbopol® 980 and Noveon® AA-1 Polycarbophil have been known to be used majorly for drug delivery applications. Hence, through this article, nanocomposites of Carbopol® 980 and Noveon® AA-1 Polycarbophil hydrogel are being brought into light as effective antibacterial hydrogels. These materials were particularly chosen because of their more relevance in pharmaceutical and biomedical applications, in formulation of buccal, vaginal, nasal, ophthalmic and rectal bioadhesive products [16,18,19].

Of late, metal nanocomposite hydrogels for antibacterial applications were developed from impregnation of nanoparticles of either monometallic or bimetallic (as alloy) [6,20-23]. However, in the present investigation bimetallic Au-core Ag-shell nanoparticles have been impregnated. Gold and silver were specifically chosen because of their gaining renewed attention for combating the threat of bacterial infection. The additional advantage is that, unlike antibiotics, metal nanoparticles (either Ag or Au) do not act via cell receptors to kill the microorganisms [24]. So, the chance of immune response in microbes to develop resistance against these nanoparticles is not possible. Hence, the problem of disease transmission/contamination through various microorganisms could be greatly eradicated without bringing any resistance in microorganisms [25].

In general, bimetallic core-shell nanoparticles were synthesized through seed-mediated growth, template synthesis, chemical reduction and laser ablation. These methods utilize not only chemical reductants but also auxiliary stabilizers, and often involved with specialized expensive

equipment and even hazardous to the environment [26]. Hence, in the present investigation extracts of naturally available mint leaves were utilized for synthesizing core-shell nanoparticles through an eco-friendly process [27-29]. This is the most appropriate and cost-effective method, which utilizes ambient conditions for nucleation of core-shell nanoparticles.

In overall, the present scientific research work involved the fabrication of Au-core Ag-shell nanocomposite hydrogels separately from two commercially available Carbopol® 980 NF and Noveon® AA-1 Polycarbophil. The possible core-shell nanoparticles were synthesized from extracts of mint leaves by an eco-friendly process. The developed nanocomposite hydrogels showed excellent swelling patterns in phosphate buffered saline (PBS), pH 7.4 solution. The antibacterial studies confirmed their excellent antibacterial efficiency. Overall, the results indicated that the developed novel nanocomposite hydrogels by eco-friendly process can be utilized for superior biomedical applications. The experimental findings pertaining to this inorganic Au-core Ag-shell nanocomposite hydrogels were presented here.

Experimental

Materials

Carbopol® 980 NF (CP) and Noveon® AA-1 Polycarbophil (NP) are obtained as gift samples from Lubrizol Advanced Materials, Europe. Acrylamide (AAm), N,N'-ethylenebisacrylamide (MBA), Ammonium Persulphate (APS), gold chloride ($HAuCl_4.xH_2O$) and silver nitrate ($AgNO_3$) were purchased from S.D. Fine-Chem Ltd., Mumbai, India. All chemicals were used without further purification. Double distilled water was used throughout the experimentation.

Preparation of the Mint leaves' extract

Mint leaves' extract was prepared following the standard procedure, similar to the methods described in our earlier study [1, 2]. In brief, fresh mint leaves were collected and thoroughly washed with double distilled water. Mint leaves broth was prepared by taking 2.5 g of thoroughly washed and finely cut mint leaves in a 500 mL Erlenmeyer flask with 100 mL of sterile double distilled water. The contents of the leaves were extracted by heating the solution at 100 ^{0}C for 2 min, cooled to room temperature and filtered through 0.45 µm PVDF Millex Filter using a 50 mL syringe. The extracted solution was preserved at 4 ^{0}C and utilized for nucleation of Au^{3+} and Ag^{+} ions.

Fabrication of hydrogels

A set of Carbopol® 980 NF hydrogels ($P(CP\text{-}AAm)_x$, x = 1-3) and Noveon® AA-1 Polycarbophil Hydrogels ($P(NP\text{-}AAm)_x$, x = 1-3) were separately fabricated by dissolving AAm (14.06 mM) and various ratios (0.05-0.15g) of acrylic acid polymers (CP/NP) in 3 mL of distilled water, stirring at 300 rpm for 2 h at 25 ^{0}C. To this aqueous solution, MBA (0.648 mM) and APS (2.191mM) were added, and the temperature was raised to 50 ^{0}C for 15min to initiate the free-radical polymerization reaction. The reaction was maintained at ambient conditions for 4 h. During the reaction period, gelation occurs leading to the formation of hydrogels. The obtained hydrogels were immersed in distilled water at room temperature for 24 h to remove unreacted materials present in the hydrogel network. Finally, various formulations of CP and NP hydrogels were dried out at ambient room temperature for 48 h. The feed compositions of the various formulated CP and NP hydrogels are presented in **Table 1.**

Fabrication of Au-core Ag-shell nanocomposite hydrogels

Approximately, 500 mg of dry hydrogels were allowed to swell in distilled water for 48 h to reach equilibrium swelling. The swollen hydrogels were transferred to a 50 mL glass beaker containing 20 mL of aqueous silver nitrate (5mM) and 10 mL of aqueous gold (III) chloride (5mM) solutions for 24 h time in order to permit equilibration. During this equilibrium stage, Ag^{+} and Au^{3+} ions were being exchanged from aqueous solution to the hydrogel networks. Finally, the ions loaded hydrogels were immersed into mint leaves' extract up to 6 h time at room temperature in order to nucleate Au^{3+} and Ag^{+} ions to Au-core Ag-shell nanoparticles. Subsequently, hydrogels with nucleated Au-core Ag-shell nanoparticles ($P(CP\text{-}AAm)_x + Ag^0 + Au^0$, x=1-3 and $P(NP\text{-}AAm)_x + Ag^0 + Au^0$, x=1-3) were dried out at ambient room temperature for 48 h and crushed for characterizations.

Characterizations

The core-shell nanocomposites were studied through morphological studies (TEM, SEM), elemental analysis (EDS), spectral analysis (FTIR), thermal analysis, swelling behavior and antibacterial test.

Transmission electron microscopy (TEM) was conducted on a JEM-1200EX, JEOL (Tokyo, Japan). The TEM sample was prepared by dispersing two to three drops (1 mg/1 mL) of finely grinded core-shell nanocomposite hydrogel solution on 3 mm copper grid and dried at ambient temperature.

Scanning electron microscopy-energy dispersive spectroscopy analysis was performed using JEOL JEM-7500F (Tokyo, Japan), operated at an accelerating voltage of 2 kV. All (SEM-EDS) samples were gold-coated, prior to examination.

The required fourier transform infrared (FTIR) spectra were recorded on a Perkin Elmer FTIR spectrometer (Model Impact 410, Wisconsin, MI, USA). Samples were examined between 500 and 4000 cm^{-1}.

Thermogravimetric analysis (TGA) of the samples were carried out using SDT Q 600 DSC instrument (T.A. Instruments-water LLC, Newcastle, DE 19720, USA) at a heating rate of 20 ^{0}C/min under a constant nitrogen flow (100 mL/min).

Swelling studies

The swelling ratio ($S_{g/g}$) of the hydrogels was determined by gravimetric method by allowing the hydrogels to swell in the Phosphate buffered saline (PBS), pH 7.4 for 24 h at 37 ^{0}C. The value of swelling ratio was calculated by using the equation, $S_{g/g} = W_s/W_d$; where, W_s and W_d denote the weight of the swollen hydrogel at equilibrium and the weight of the dry hydrogel, respectively [21,22]. The data provided was an average value of 3 individual readings of samples.

Antibacterial test

The antibacterial activity was tested against *E. coli* (G -) and *B. Subtilis* (G +). The method followed was 'Disc diffusion method', as described in the literature. The required nutrient agar medium was prepared by mixing peptone (5.0 g), beef extract (3.0 g), sodium chloride (5.0 g) and agar (15.0 g) in 1000 mL of distilled water and the pH was adjusted to 7.0. The agar medium was sterilized in a conical flask at a pressure of 6.8 kg (15 lbs) for 30 min and transferred into sterilized petri dishes in a laminar air flow chamber (Microfilt Laminar Flow Ultra Clean Air Unit, Mumbai, India) for solidification. Later, 50µL of microbial culture was uniformly streaked over the solid surface. To this inoculated Petri dish, pre-impregnated discs

with a standard gel concentration (20 mg/10 mL distilled water) were placed and incubated at 37 ^{0}C for 48 h to obtain inhibition zones. Finally, the formed inhibition zones were measured and photographed.

Results and discussions

In the present investigation, Carbopol® 980 NF (CP) and Noveon® AA-1 Polycarbophil (NP) were successfully utilized to fabricate hydrogels. During the typical polymerization process, gelation occurs through linking acrylamide (AAm) to form initially the polydisperse soluble branched polymers of acrylamide called 'sol'. The process of linking leads the branched acrylamide polymer to increase its size to form an insoluble infinite polymer with interpenetrating CP/NP molecular chains called 'gel' or 'network'. The transition of a system from finite branched polymers to infinite polymer is called 'sol-gel transition' (or 'gelation') and the critical point where gel first appears is called 'gel point' [30]. Once the hydrogels were formed, bimetallic Au-core Ag-shell nanoparticles were impregnated into the gel network by swelling method [2]. Core-shell metal nanoparticles that produced by chemical reducing agents are usually associated with environmental toxicity or biological hazards. From this perceptive, extracts of naturally occurring mint leaves were chosen for the nucleation of core-shell nanoparticles. The successfully fabricated inorganic Au-core Ag-shell nanocomposite hydrogels *via* eco-friendly green process was pictorially presented in **Scheme 1**.

Mechanism of Au-core Ag-shell formation

Mint leaves' extracts containing hydroxyl groups (–OH) associated with menthol (major component present in mint extracts) offer sufficient reduction capacities for reduction of metal ions (Ag^+ and Au^{3+}) [31]. In a competitive process involving both silver ions and gold ions, the

reduction of gold ions occurs first than silver ions [28]. The comparatively slower reduction rate of silver ions relative to that of gold ions is due to the differences in their reduction potentials. The redox potential being considerably lower for Ag^{+} to Ag^{0} (E^{o} = + 0.80 V) than Au^{3+} to Au^{0} (E^{o} = +1.50 V) allows gold ions to reduce first than silver ions (equations shown (1) and (2)) [28]. Once, gold ions are reduced, the surrounded by silver ions eventually get reduced and deposit over reduced Au^{3+} (i.e. Au^{0}) in the form of layer, giving Au-core and Ag-shell nanoparticles [28]. Further, size reduction to nano dimension increases not only the surface energy but also number of binding sites between Au and Ag atoms. This stabilizes the total energy of each individual core-shell nanoparticle [32]. Hence, the formation of bimetallic Au-core and Ag-shell nanoparticles might be explained by the combination of these factors involving balance between the binding energy and the surface energy.

$$Ag^{+} + \bar{e} \longrightarrow Ag^{0}, E^{o} = + 0.80 \text{ V (Slower reduction)} \quad (1)$$

$$Au^{3+} + 3\bar{e} \longrightarrow Au^{0}, E^{o} = + 1.50 \text{ V (Faster reduction)} \quad (2)$$

Evidence for successful formation of core-shell nanoparticles was confirmed by transmission electron microscopy (TEM) analysis. The TEM images of the core-shell nanoparticles are shown in **Fig 1**. Similar to the observation of many research groups, a boundary between Au and Ag elements can be distinguished by bright and dark contrast, where the dark portion was assumed to be core (Au) and bright portion was assumed to shell (Ag) [33]. The additional information revealed by TEM data inferred that the nanoparticles formed were within nano dimension of ~15 ± 3 nm and without any aggregation. It may be predicted that the core-shell nanoparticles were highly stabilized through the available hydrophilic functional groups of the hydrogel network [21]. Hence, core-shell nanoparticles without aggregation were

formed. The formation of core-shell was supported by scanning electron microscopy-energy dispersive spectroscopy (SEM-EDS) analysis. The SEM-EDS images of core-shell nanocomposite hydrogels, P(CP-AAm)$_3$ + Ag^0 + Au^0 **(Fig 2A(c))** and P(NP-AAm)$_3$ + Ag^0 + Au^0 **(Fig 2B(c))** showed signals corresponding to Au and Ag in the spectra, indicating the core-shell was composed of Au and Ag [29, 34]. Further, the morphological studies through SEM examination showed a clear surface pattern for pure P(CP-AAm)$_3$ hydrogel (**Fig 2A(a)**) and P(NP-AAm)$_3$ hydrogel (**Fig 2B(a)**), and nanoparticles distribution pattern for core-shell nanocomposite hydrogels (P(CP-AAm)$_3$ + Ag^0 + Au^0**(Fig 2A(b))** and P(NP-AAm)$_3$ + Ag^0 + Au^0 **(Fig 2B(b))**. This supports the presence of core-shell nanoparticles in the hydrogel network.

The evidence for the successful preparation of Au-core Ag-shell nanocomposite hydrogel was analyzed through hydrogel–core-shell nanoparticles interaction from FTIR spectral data, as shown in **Fig 3**. The FTIR spectra of pure P(CP-AAm)$_3$ and core-shell nanocomposite of P(CP-AAm)$_3$ + Ag^0 + Au^0 are presented in **Fig 3A**. The spectrum of P(CP-AAm)$_3$ hydrogel showed absorption bands at 3335 cm^{-1} and at 3190 cm^{-1} corresponding to –OH and –NH groups stretching vibrations respectively [3,4]. The other important bands at 2924 cm^{-1}, 1643 cm^{-1}, 1184 $cm^{-1}$and 1114 cm^{-1} were assigned to stretching vibrations of –C–H, carbonyl and –C–O groups respectively present in P(CP-AAm)$_3$ hydrogel [22,35]. These peaks were shifted in case of P(CP-AAm)$_3$ + Ag^0 + Au^0 due to interactions of the core-shell nanoparticles with the functional groups of the hydrogel. The FTIR spectra of pure P(NP-AAm)$_3$ and core-shell nanocomposite of P(NP-AAm)$_3$ + Ag^0 + $Au^0$are presented in **Fig 3B**. For pure P(NP-AAm)$_3$, absorption bands at 3330 cm^{-1} and at 3182 cm^{-1} corresponding to –OH and –NH groups stretching vibrations respectively [3,4]. The other important bands at 2932 cm^{-1}, 1644 cm^{-1}, 1181 $cm^{-1}$and 1119 cm^{-1} were assigned to stretching vibrations of –C–H, carbonyl and –C–O groups respectively present in P(NP-

$AAm)_3$ hydrogel [22,35]. These peaks were shifted in the case of $P(NP\text{-}AAm)_3 + Ag^0 + Au^0$ as noticed in the earlier case. Over all, the shifting of peaks confirms the interactions of the core-shell nanoparticles with the functional groups of the hydrogel.

Thermo gravimetric analysis (TGA), another piece of evidence, indicates simultaneously the existence of core-shell nanoparticles within the three dimensional (3D) networks of hydrogel and the thermal stability of the hydrogels. As shown in TGA curves (**Fig 4A**), at 700 ^oC, pure $P(CP\text{-}AAm)_3$ (**Fig 4A(a)**) and pure $P(NP\text{-}AAm)_3$ (**Fig 4A(b)**) degrade almost completely but the core-shell nanocomposite hydrogels remain with residue masses. The residue mass leftovers of the nanocomposites: $P(CP\text{-}AAm)_1$ (1.86 %), $P(CP\text{-}AAm)_3$ (4.77 %), $P(NP\text{-}AAm)_1$ (2.58 %) and $P(NP\text{-}AAm)_3$ (6.58 %) clearly indicate the existence of inorganic Au-core Ag-shell nanoparticles internally in the 3D networks of hydrogels. Thermal studies led to the conclusion that with the increase in the percentage (%) of CP and NP, the residue mass leftovers increase. This was due to the rise in nanoparticles number, occurred due to the strong bonding characteristics developed among nanoparticles and the acrylic acid polymers with the increase of CP and NP concentrations. The phenomenon can be comparable with Ag or Au impregnated nanocomposite systems [1,2,36]. In over all, the TGA data concludes that both the nanocomposite hydrogels and the pure hydrogels show almost similar pattern of curves indicating no significant difference in the thermal stability. The residual mass of the nanocomposite leftovers at the temperature over 700 ^oC is actually the mass of the core-shell nanoparticles been fabricated in the hydrogels.

Swelling studies

Swelling studies is a characteristic analysis used to determine 'Swelling property' or 'swelling ratio' of the developed hydrogels. 'Swelling property' or 'swelling ratio' is a

characteristic parameter, indicates the absorption capacity of a functional material for blood, bodily fluids and secretion exudates from injured wounds.

In the present investigation, it was noticed that the value of swelling ratio of the developed nanocomposite hydrogels ranges from: 12 to 22 (g/g), indicating that they can absorb blood or any other bodily fluids to an extent of 1200-2200% to its dry weight (shown in **Fig 4B(a)** and **Fig 4B(b)**). Further, the value of the swelling ratio was proportional to the concentration of CP/NP. From swelling ratio data, it was also evident that with the increase in CP/NP concentration, the value of swelling ratio also increases. The observed phenomenon was due to the hydrophilic nature of the developed CP/NP hydrogel [1]. Further, core-shell nanocomposite hydrogels show higher swelling ratio than respective pure P(CP-AAm) hydrogels (**Fig 4B(a)**) and pure P(NP-AAm) hydrogels (**Fig 4B(b)**). The reason being that, when Au^{3+} and Ag^{+} ions loaded hydrogels were treated with mint leaves' extract, nucleation of ions occurs resulting in the formation of core-shell nanoparticles. This allows the hydrogel to expand 3D networks and promote higher water molecules uptake capacity [1,2]. One more reason for the expansion of 3D networks was 'size factor'. Nanoparticles formed with varying nanodimension results in the acquisition of different surface charges over their surfaces, this cause absolute expansion of the networks [4].

The overall swelling data significantly confirmed that the developed hydrogels were good absorbents for blood, bodily fluids and secretion exudates from injured wounds or other body parts.

Antibacterial activity

Devastation of bacteria is the key parameter that determines the utility of the developed hydrogels for various applications in bacterial prone areas. The efficiency of the developed nanocomposite hydrogels against bacteria was determined by conducting antibacterial activity against *E. coli* (G -) and *B. subtilis* (G +), shown in **Fig 5**. The results revealed a strong reduction in the number of bacterial colonies around core-shell nanocomposite samples. The mechanism of growth inhibitory effect of nanoparticles against the microorganisms is not clear so far [37]. However, among the various possible mechanisms proposed by many authors, 'Inhibition by formation of pits,' was considered to be suitable here. It was assumed that the interaction of nanoparticles with bacteria results in the formation of pits over the cell wall of the bacterial membrane. These pits cause the leakage of biologically important lipopolysaccharide molecules and membrane proteins, leading to microbial death [38-41]. Though the shell of the core-shell nanoparticles that interacts with the cell wall of the bacterial membrane comprises silver atoms, the efficiency of bacterial inhibition is incomparable with silver nanoparticles because Au-core Ag-shell nanoparticles show enhance antibacterial activity. This was proven by Banerjee et al [42]. The enhanced antibacterial properties of Au-core Ag-shell nanoparticles was possibly due to the more active silver atoms in the shell surrounding Au-core due to high surface free energy of the surface silver atoms owing to shell thinness in the bimetallic nanoparticle structure.

The diameter of the inhibition zone exhibited by the optimized nanocompsite hydrogel samples aganist *E. coli* and *B. subtilis* was found to be in the range 14.2–17 mm. The diameter of the inhibition zones of P(CP-AAm)$_3$ + Ag^0 + Au^0 and P(NP-AAm)$_3$ + Ag^0 + Au^0 against *E. coli* are 15.8 mm and 17.0 mm, and against *B. subtilis* are 14.2 mm and 15.1 mm respectively. These results are quite expected and seemed to be followed according to the nanoparticles content in the hydrogel matrixes. It was evident from the TGA analysis that the percentage of nanoparticles

content had been found higher for P(NP-AAm)$_3$ + Ag^0 + Au^0 (6.58 %) than P(CP-AAm)$_3$ + Ag^0 + Au^0 (4.77 %). Hence, inhibition zones were observed higher for P(NP-AAm)$_3$ + Ag^0 + Au^0 than P(CP-AAm)$_3$ + Ag^0 + Au^0 [36]. Further, according to the Standard Antibacterial test "SNV 195920–1992", specimens showing more than 1 mm microbial zone inhibition can be considered as good antibacterial agents [43]. Hence, the novel inorganic Au-core Ag-shell nanocomposite hydrogels developed from eco-friendly green process can be considered as good antibacterial agents, effective in killing the bacteria.

Conclusion

Antibacterial nanocomposite hydrogels of Au-core Ag-shell were fabricated from medically importance gained Carbopol® 980 NF (CP) and Noveon® AA-1 Polycarbophil (NP) acrylic acid polymeric matrices. The process adopted was eco-friendly process, where natural mint leaves' extract, free from toxic chemicals were successfully utilized to synthesize Au-core Ag-shell nanoparticles. The developed nanocomposite hydrogels showed excellent antibacterial activity against *E.coli* (G -) and *B. subtilis* (G +) and also exhibited pronounced swelling properties. Hence, from the view point of applications, the developed hydrogels may be utilized for superior biomedical applications ranging from designing wound dressing materials to sanitary appliances like: incontinence articles, tampons, nappy pants, nappy liners and sanitary napkins.

Acknowledgement

The author (IF 110192) wish to acknowledge the Department of Science & Technology (DST, INIDA) and the Ministry of Science & Technology, for providing the financial assistance

through the Innovation in Science Pursuit for Inspired Research programme (INSPIRE).The author KVP wishes to acknowledge the CIPA, CONICYT Regional, GORE BIO-BIO R08C1002

References

1. T. Jayaramudu, G. M. Raghavendra, K. Varaprasad, R. Sadiku and K. M. Raju, *Carbohydr. Polym.*, 2013, **92**, 2193-2200.
2. T. Jayaramudu, G. M. Raghavendra, K. Varaprasad, R. Sadiku, K. Ramam and K. M. Raju,*Carbohydr. Polym.*, 2013, **95**, 188– 194.
3. N. N. Reddy, Y. M. Mohan, K. Varaprasad, S. Ravindra, P. A. Joy and K. M. Raju, *J. Appl. Polym. Sci.*, 2011, **122**, 1364–1375.
4. N. Narayana Reddy, K. Varaprasada, S. Ravindra, G. V. Subba Reddy, K. M. S. Reddy, K. M. M. Reddy and K. M. Raju, *Colloids Surf., A: Physicochem. Eng. Aspects*, 2011, **385**, 20– 27.
5. N. N. Reddy, Y. M. Mohan, K. Varaprasad, S. Ravindra, K. Vimala, P. A. Joy and K. M. Raju, *J Polym Res.*, 2011, **18**, 2285–2294.
6. K. Varaprasad, Y. M. Mohan, S. Ravindra, N. N. Reddy, K. Vimala, K. Monika, B. Sreedhar and K. Mohana Raju, *J. Appl. Polym. Sci.*, 2010, **115**, 1199–1207.
7. N. A. Peppas and A. G. Mikos, *Hydrogels in Medicine and Pharmacy*, CRC Press, Boca Raton, FL, 1986, **1**, 1–27.
8. L. Brannon-Peppas, *Absorbent Polymer Technology*, Elsevier, Amsterdam, 1990, 45–66.
9. N. A. Peppas, P. Bures, W. Leobandung and H. Ichikawa, *Eur. J. Pharm. Biopharm.*, 2000, **50**, 27–46.
10. S. Benamer, M. Mahlous, A. Boukrif, B. Mansouri and S. L. Youcef, *Nucl. Instrum. Methods Phys. Res., Sect. B*, 2006, **248**, 284–290.

11. Y. C. Nho, S. E. Park, H. I. Kim, and T. S. Hwang. *Nucl. Instrum. Methods Phys. Res., Sect. B*, 2005, **236**, 283–288.

12. J. M. Rosiak, P. Ulanski and A. Rzeinicki, *Nucl. Instrum. Methods Phys. Res., Sect. B*, 1995, **105**, 335-339.

13. J. M. Rosiak and F. Yoshii, *Nucl. Instrum. Methods Phys. Res., Sect. B*, 1999, **151**, 56-64.

14. G. C. Maity, J. Phys. Sci., 2008, **12**, 173-186.

15. S. Q. Liu, R. Tay, M. Khan, P. L. R. Ee, James L. Hedrickc and Y. Y. Yang, *Soft Matter*, 2010, **6**, 67-81.

16. S. Gupta, M. K. Samanta and A. M. Raichur, *AAPS PharmSciTech*, 2010, **11**, 322–335.

17. M. Kerec, M. Bogataj, B. Mugerle, M. Gasperlin and A. Mrhar, *Int. J. Pharm*., 2002, **241**, 135–143.

18. N. Aggarwal, S. Goindi and S. D. Mehta, *AAPS PharmSciTech*, 2012, **13**, 67–74.

19. M. T. Islam, N. Rodríguez-Hornedo, S. Ciotti and C. Ackermann, *AAPS J*., 2004, **6**, 35.

20. Y. M. Mohan, K. Vimala, V. Thomas, K. Varaprasad, B. Sreedhar, S. K. Bajpai and K. M. Raju, *J. Colloid Interface Sci.*, 2010, **342**, 73–82.

21. P. S. K. Murthy, Y. M. Mohan, K. Varaprasad, B. Sreedhar and K. M. Raju, *J. Colloid Interface Sci.*, 2008, **318**, 217–224.

22. K. Varaprasad, Y. Murali Mohan, K. Vimala and K. M. Raju, *J. Appl. Polym. Sci.*, 2011, **121**, 784–796.

23. P. R. Reddy, K.Varaprasad, N. Narayana Reddy, K. M. Raju and N. S.Reddy, *J. Appl. Polym. Sci.*, 2012, **125**, 1357–1362.

24. N. S. Z. Haider, U. Kiran, I. M. Ali, A. Hameed and S. A. N. Ali, Brno, Czech Republic, EU, 2012, **10**, 23 – 25.

25. T. Ristic, L. Z. Zemljic, M. Novak, M. K. Kuncic, S. Sonjak, N. G. Cimerman and S. Strnad, *Science against microbial pathogens: communicating current research and technological advances*, Ed. A. Méndez-Vilas, 2011, 36-51.
26. G. Zhan, J. Huang, M. Du, I. Abdul-Rauf, Y. Ma and Q. Li, *Mater. Lett*., 2011, **65**, 2989–2991.
27. D. S. Shenya, J. Mathewa and D. Philip, *Spectrochim. Acta, Part A*, 2011, **79**, 254–262.
28. S. S. Shankar, A. Rai, A. Ahmad and M. Sastry, *J. Colloid Interface Sci*., 2004, **275**, 496–502.
29. A. Rai, M. Chaudhary, A. Ahmad, S. Bhargava and MuraliSastry, *Mater. Res. Bull*., 2007, **42**, 1212–1220.
30. M. Rubinstein and R. H. Colby, Polymer Physics, *Oxford University Press*, Oxford, 2003.
31. S. Ravindra, Y. M. Mohan, N. N. Reddy and K. M. Raju, *Colloids Surf., A: Physicochem. Eng. Aspects,* 2010, **367**, 31–40.
32. K. Hirakawa, *in Smart Nanoparticles Technology*, Ed. A Hashim, 2012, ISBN: 978-953-51-0500-8.
33. S. Pyne, P. Sarkar, S. Basu, G. P. Sahoo, D. K. Bhui, H. Bar and A. Misra, *J Nanopart*., 2011, **13**, 1759–1767.
34. T. Li, S. Chattopadhyay, T. Shibata, R. E. Cook, J.T. Miller, N. Suthiwangcharoen, S. Lee, R. E. Winansa and B. Lee, *J. Mater. Chem*., 2012, 22, 14458–14464.
35. K. Vimala, Y. Murali Mohan, K. Samba Sivudu, K. Varaprasad, S. Ravindra, N. Narayana Reddy, Y. Padma, B. Sreedhar and K. M. Raju, *Colloids Surf., B*, 2010, **76**, 248–258.

36. G. M. Raghavendra, T. Jayaramudu, K. Varaprasad, R. Sadiku, S. Sinha Ray and K. M. Raju, *Carbohydr. Polym.*, 2013, **93**, 553– 560.

37. H. H. Lara, E. N. Garza-Treviño, L. Ixtepan-Turrent and K. S. Dinesh, *J Nanobiotechnology*, 2011, 9:30.

38. N. A. Amro, L. P. Kotra, K. Wadu-Mesthrige, A. Bulychev, S. Mobashery and G. Liu, *Langmuir*, 2000, **16**, 2789-2796.

39. A. Nasrollahi, Kh. Pourshamsian and P Mansourkiaee, *Int.J.Nano.Dim*, 2011, **1**, 233-239.

40. M. F. Zawrah and S. I. A. El-Moez, Life Sci. J., 2011, **8**, 37-44.

41. M. Singh, S. Singh, S. Prasada and I. S. Gambhir, *Dig. J. Nanomater and Bios*, 2008, **3**, 115-122.

42. M. Banerjee, S. Sharma, A. Chattopadhyay and S. S. Ghosh, *Nanoscale*, 2011, **3**, 5120-5125.

43. G. M. Raghavendra, T. Jayaramudu, K. Varaprasad, S. Ramesh and K. M. Raju, *RSC Adv.*, 2014, **4**, 3494–3501.

Caption for Scheme

Scheme 1: Pictorial representation of facile eco-friendly fabrication of antibacterial nanocomposite hydrogels.

Caption for Figures

Fig 1: TEM images of core-shell nanoparticles present in hydrogel nanocomposites of: A) P(CP-AAm)$_3$; B) P(NP-AAm)$_3$ with (a) lower magnification and (b) higher magnification.

Fig 2: SEM images of A) (a) pure P(CP-AAm)$_3$ hydrogel, (b) P(CP-AAm)$_3$ + Ag^0 + Au^0 hydrogel; B) (a) pure P(NP-AAm)$_3$ hydrogel, (b) P(NP-AAm)$_3$ + Ag^0 + Au^0 hydrogel and SEM-EDS image of A) (c) P(CP-AAm)$_3$ + Ag^0 + Au^0 hydrogel; B) (c) P(NP-AAm)$_3$ + Ag^0 + Au^0 hydrogel.

Fig 3: FTIR spectra of A) pure P(CP-AAm)$_3$ hydrogel, P(CP-AAm)$_3$ + Ag^0 + Au^0 hydrogel; B) pure P(NP-AAm)$_3$ hydrogel, P(NP-AAm)$_3$ + Ag^0 + Au^0 hydrogel.

Fig 4: A) Thermo-gravimetric analysis of: (a) pure P(CP-AAm)$_3$ hydrogel, P(CP-AAm)$_3$ + Ag^0 + Au^0 hydrogel and (b) pure P(NP-AAm)$_3$ hydrogel, P(NP-AAm)$_3$ + Ag^0 + Au^0 hydrogel; B) Swelling ratio of pure and core-shell nanocomposite hydrogels of (a) P(CP-AAm), (b) pure P(NP-AAm).

Fig 5: Antibacterial activity of: (a)P(CP-AAm)$_3$ + Ag^0 + Au^0 hydrogel, (b) P(NP-AAm)$_3$ + Ag^0 + Au^0 hydrogel, (c) pure P(CP-AAm)$_3$ + pure P(NP-AAm)$_3$ against: A) *E. coli;* B) *B. subtilis*.

Caption for Table

Table 1: Feed compositions of various formulated CP and NP hydrogels.

Scheme 1: Pictorial representation of facile eco-friendly fabrication of antibacterial nanocomposite hydrogels
582x226mm (72 x 72 DPI)

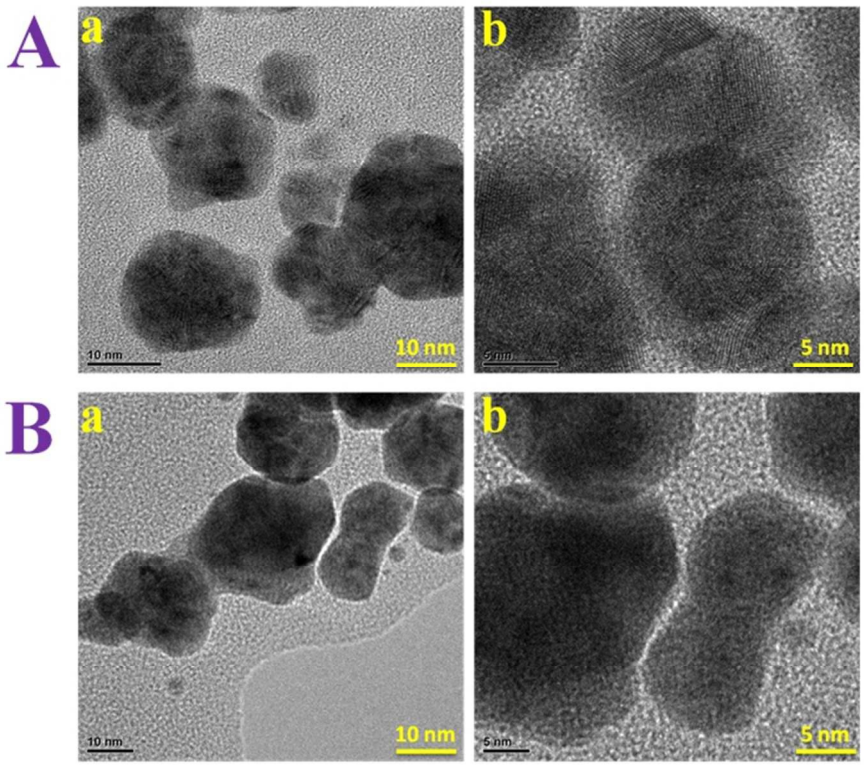

Fig. 1: TEM images of core-shell nanoparticles present in hydrogel nanocomposites of: A) P(CP-AAm)3; B) P(NP-AAm)3 with (a) lower magnification and (b) higher magnification
299x237mm (72 x 72 DPI)

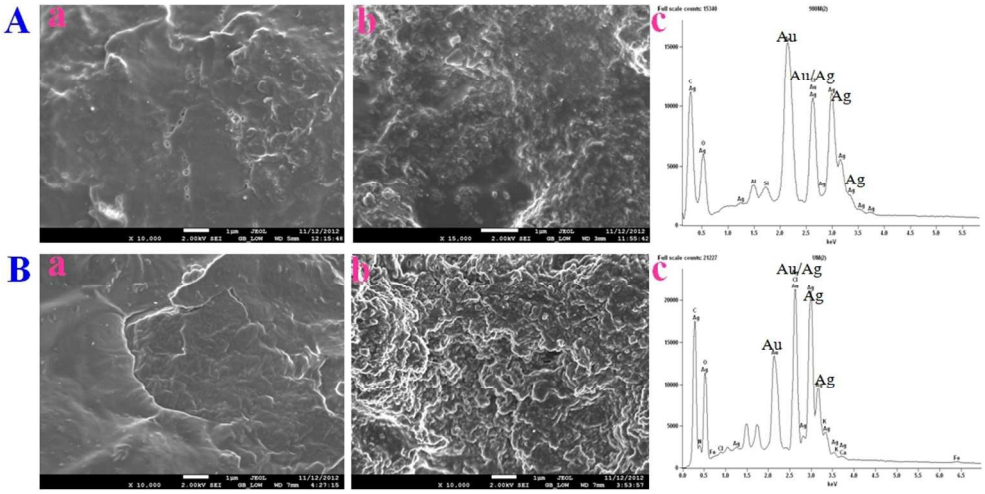

Fig. 2: SEM images of A) (a) pure P(CP-AAm)3 hydrogel, (b) P(CP-AAm)3 + Ag0 + Au0 hydrogel; B) (a) pure P(NP-AAm)3 hydrogel, (b) P(NP-AAm)3 + Ag0 + Au0 hydrogel and SEM-EDS image of A) (c) P(CP-AAm)3 + Ag0 + Au0 hydrogel; B) (c) P(NP-AAm)3 + Ag0 + Au0 hydrogel
408x209mm (72 x 72 DPI)

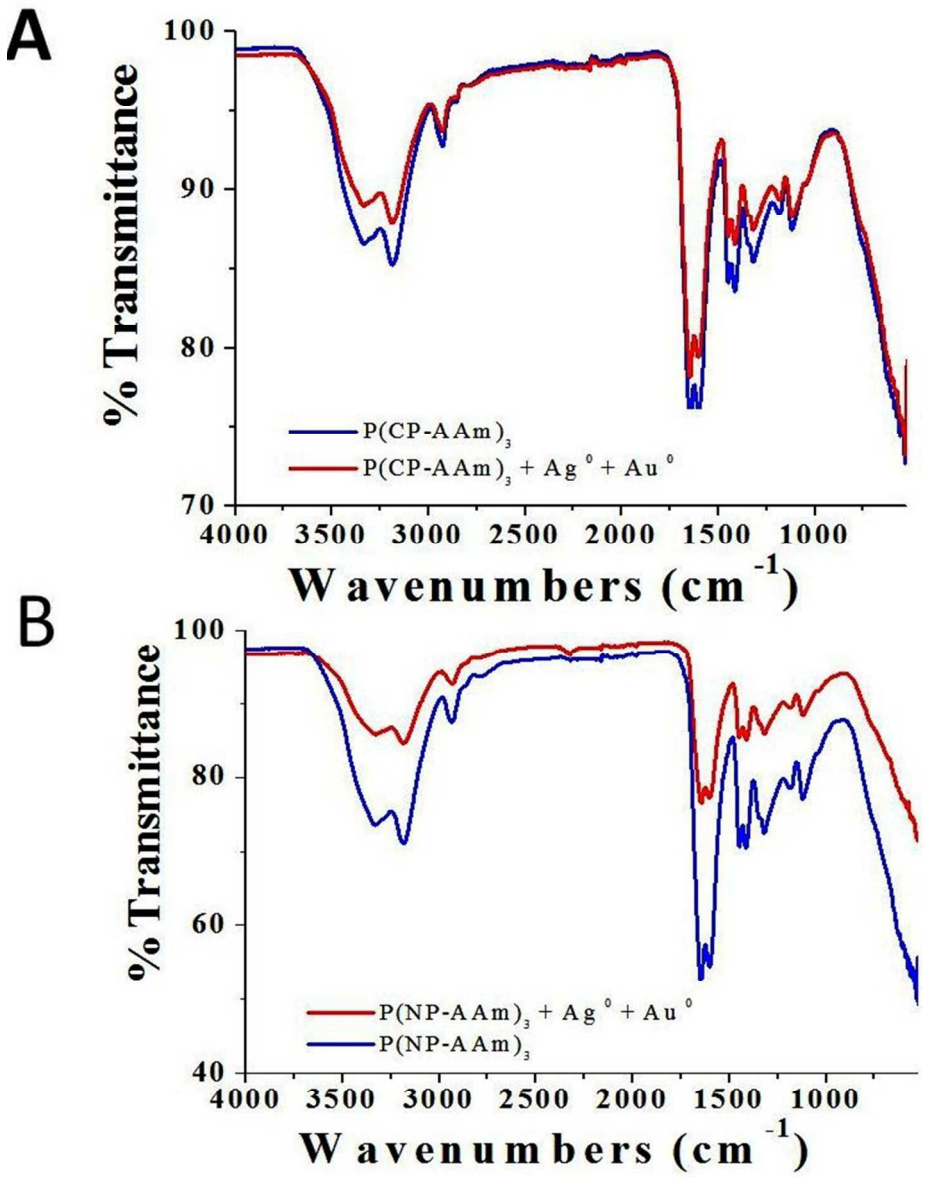

Fig. 3: FTIR spectra of A) pure P(CP-AAm)3 hydrogel, P(CP-AAm)3 + Ag0 + Au0 hydrogel; B) pure P(NP-AAm)3 hydrogel, P(NP-AAm)3 + Ag0 + Au0 hydrogel
194x255mm (96 x 96 DPI)

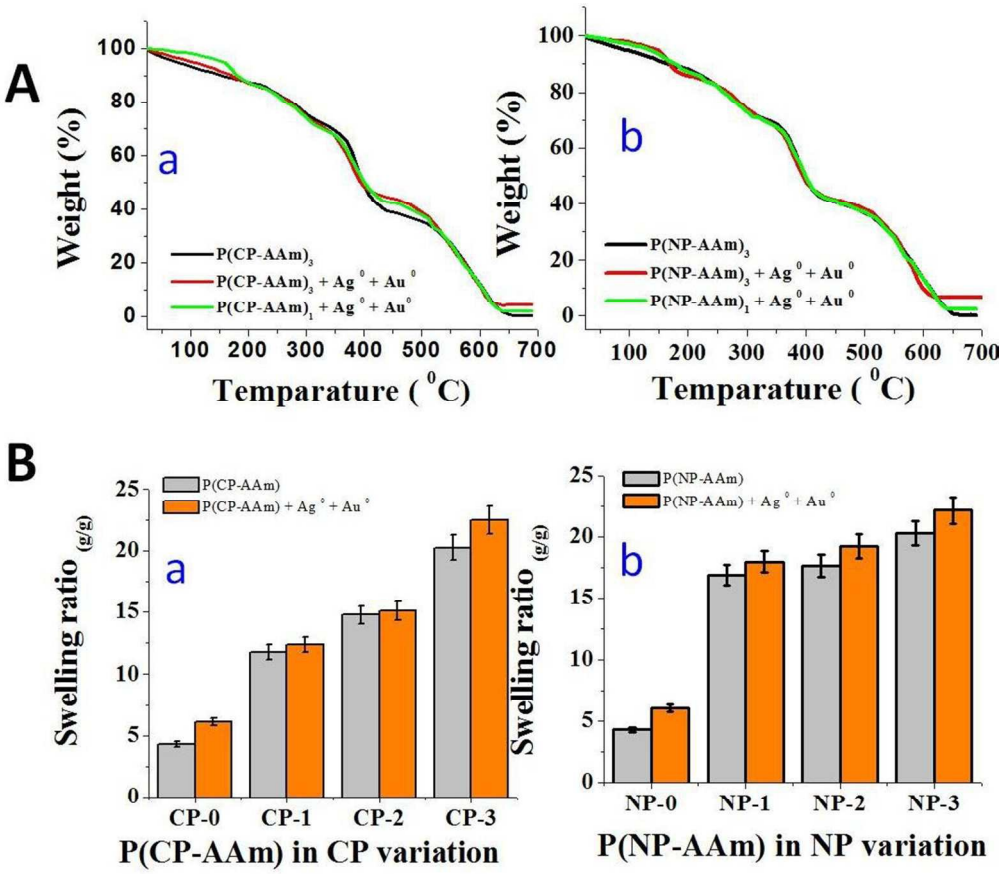

Fig. 4
284x254mm (96 x 96 DPI)

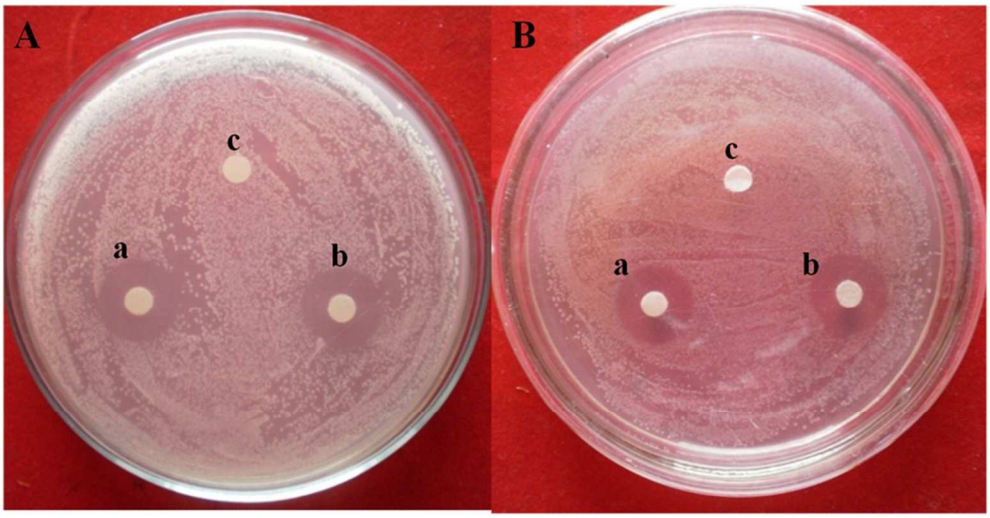

Fig. 5: Antibacterial activity of: (a) P(CP-AAm)3 + Ag0 + Au0 hydrogel, (b) P(NP-AAm)3 + Ag0 + Au0 hydrogel, (c) pure P(CP-AAm)3 + pure P(NP-AAm)3 against: A) E. coli; B) Bacillus.
341x176mm (72 x 72 DPI)

Hydrogel code	AAm (mM)	CP (g)	NP (g)	MBA (mM)	APS (mM)
P(AAm)	14.06	0.0	0.0	0.648	2.191
P(CP-AAm)$_1$	14.06	**0.05**	0.0	0.648	2.191
P(CP-AAm)$_2$	14.06	**0.10**	0.0	0.648	2.191
P(CP-AAm)$_3$	14.06	**0.15**	0.0	0.648	2.191
P(NP-AAm)$_1$	14.06	0.00	**0.05**	0.648	2.191
P(NP-AAm)$_2$	14.06	0.00	**0.10**	0.648	2.191
P(NP-AAm)$_3$	14.06	0.00	**0.15**	0.648	2.191